Available online at www.sciencedirect.com
ScienceDirect
International Journal of Multiphase Flow 34 (2008) 303–311
International Journal of Multiphase Flow
www.elsevier.com/locate/ijmulflow

Two-phase flow pattern identification using continuous hidden Markov model

Ali Mahvash, Annie Ross *

Department of Mechanical Engineering, École Polytechnique de Montréal, C.P. 6079, Succ. Centre-Ville, Montréal (Qué), Canada H3C 3A7

Received 3 January 2007; received in revised form 6 June 2007

Abstract

This paper presents a new method for identifying two-phase flow regimes from the instantaneous local fluid phase signals using continuous hidden Markov model (CHMM). CHMM is known to be a very strong pattern identifier. Air–water two-phase flows were realized in a transparent vertical tube. The tube length was 2 m, and its inner diameter was 19 mm. The instantaneous local fluid phase signals were collected using a single step index multimode optical fiber probe located at the center and mid-length of the tube. Signal features required in CHMM implementation were extracted using an innovative method. Various aspects of hidden Markov modeling and their effects on the results were studied. The flow pattern results are in very good agreement with photographs of the flow captured during the experiments. In sum, the results show that hidden Markov model has a good potential in identifying two-phase flow patterns.

Keywords: Pattern identification; Two-phase flow; Hidden Markov model; Optical probe

1. Introduction

Two-phase flows very often exist in industrial applications such as filtration, lubrication, spray processes, natural gas networks and nuclear reactor cooling. In the study of two-phase flow, flow regimes indicate how the phases are distributed and mixed due to the physical nature of the system. Two-phase flow regimes depend on the type of fluid–fluid combination, the flow rates and direction, the conduit shape, size and inclination. Further, heat and mass transfer rates, momentum loss, rate of back mixing and pipe vibration all vary greatly with the flow regimes. Hence, it is quite important and necessary to recognize the regimes and discern their relationship with the flow properties.

Many experimental and theoretical researches have been done in this area and as a result, there are several classification methods, and several two-phase flow regime maps. The early experimental works were mostly based on direct observations. High-speed photography technique, X-ray attenuation picture and suchlike are some of the methods in which the flow regimes are detected from direct observations. Although these methods are inexpensive and, in most cases, easy to perform, they are to a great extent subjective. Furthermore, in order to increase the objectivity, indirect methods were developed. Indirect observation methods deal with the fluctuating properties of two-phase flow. Such fluctuations can be observed in the local pressure, the instantaneous two-phase mixture ratio, and suchlike. It has been stated that there is a correlation between flow regimes and the fluctuation characteristics of the two-phase flow properties (Rouhani and Sohal, 1983; Das and Pattanayak, 1993). Thus, in most cases, mathematical and statistical models are used to analyze these fluctuation characteristics and to determine the flow regime. Indirect observation methods include pressure fluctuation analysis, X-ray attenuation fluctuation analysis, electrical impedance method, and so on (Rouhani and Sohal, 1983).

* Corresponding author. Tel.: +1 514 340 4711x4591; fax: +1 514 340 4176.
E-mail address: annie.ross@polymtl.ca (A. Ross).

0301-9322/$ - see front matter © 2007 Elsevier Ltd. All rights reserved.
doi:10.1016/j.ijmultiphaseflow.2007.08.006

Experimental methods are rather effective for detecting clearly established flow regimes. However, in conditions close to a transition between two regimes, detecting the flow regime is crucially difficult and most works were done on theoretical bases. In these methods, mechanisms of transition in two-phase flow are analyzed using theoretical models. Then, for any possible transition between regimes, a criterion is found and using these criteria, flow regime maps were depicted. The map derived from the work of Taitel et al. (1980) is one of those that are based on theoretical models. Further, due to the complex nature of two-phase flow, theoretical analyses have not been able to describe the system perfectly. Therefore, a technique is still required which, whether experimentally or theoretically, will detect and describe the flow regime in conditions near regime transitions.

In this research, a new method is developed for identifying internal two-phase flow regimes, from the instantaneous local fluid phase signals obtained using an optical fiber probe system inside a vertical channel. The basic idea of this method is to detect flow regimes through signal pattern analysis. As mentioned, there is a correlation between the fluctuation characteristics of two-phase flow properties and the flow regimes. Moreover, the signals are interpretations of such fluctuating properties. Therefore, the signal patterns can be considered as representatives of the flow patterns. By analyzing and distinguishing these signal patterns, the flow patterns can be detected, and flow regimes can be identified. In most of the previous methods of this type, statistical properties such as probability density function (PDF) (Jones and Zuber, 1975; Vince and Lahey, 1982; Kelessidis and Dukler, 1989; Costigan and Whalley, 1997) were used for detecting flow patterns. In these methods, the statistical features of a given fluctuating property of the flow were obtained for each regime and were then used for comparing different regimes. In the present work, signal patterns were analyzed in an enhanced and objective manner using hidden Markov models (HMM), and flow regimes were recognized through flow patterns.

2. Flow pattern classification

According to Taitel et al. (1980), flow regimes for an upward gas–liquid flow in a vertical conduit can be categorized as follows (Fig. 1):

Bubbles (Fig. 1a): This flow regime occurs at low gas flow rates where the gas phase is approximately uniformly distributed in the form of discrete bubbles in a continuum of liquid phase. Large deformable bubbles rise with a zigzag motion. Occasional Taylor-type bubbles can also be observed.

Finely dispersed bubbles (Fig. 1b): At higher velocities, the large bubbles break up due to turbulent forces. The bubbles come in smaller and more dispersed spheres in comparison with the bubbly flow. They behave as non deformable spheres.

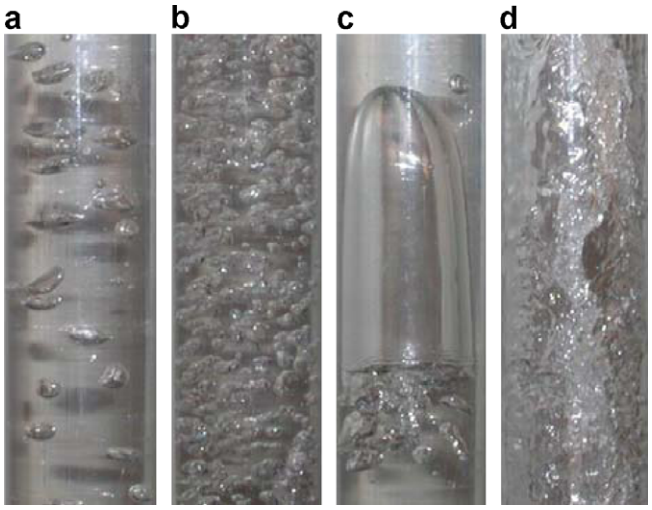

Fig. 1. Two-phase upward flow patterns in a vertical tube: (a) dispersed bubbles, (b) finely dispersed bubbles, (c) slugs, and (d) churns.

Slug flow (Fig. 1c): In this case, most of the gas appears in large bullet shaped bubbles, also known as Taylor bubbles, which have a diameter almost equal to the pipe diameter. The liquid slug area between two Taylor bubbles is filled with small bubbles that are very similar to those in bubbly flow.

Churn flow (Fig. 1d): Churn flow is a highly disordered flow that happens at high gas flow rates because of instabilities in the slugs. Churn flow can be interpreted as an irregular, chaotic and disordered slug flow. It is also characterized by an oscillatory flow, with the liquid phase moving alternately upward and downward in the channel.

Annular flow (not depicted): At higher gas flow rates, the oscillations of the churn flow disappear, and there is a continuum of gas at the center of the pipe. The liquid phase is continuously flowing upward, and it is distributed between a liquid film, which is on the pipe wall, and a dispersion of droplets in the gas core of the flow.

3. Hidden Markov models

An HMM is a doubly embedded stochastic process, which has a rich mathematical structure. HMMs have been proven to be very strong pattern identifiers with a good accuracy on most critical applications. HMMs have been used in speech recognition starting from the 1960s. Rabiner (1989) published an insightful tutorial on HMMs and their application in speech recognition. Since then, HMMs have been used in many other fields including mechanical engineering related fields such as tool wear monitoring (Ertunc et al., 2001; Wang et al., 2002), robotics (Hannaford and Lee, 1991) and faults diagnosis (Lee et al., 2004; Bunks et al., 2000; Ocak and Loparo, 2005). In this paper, some basic HMM concepts are briefly introduced to provide the reader with a general understanding of the modeling and identification process. A comprehensive and well

detailed description on HMMs can be found in Rabiner's tutorial.

HMM is an extension to a Markov process. A Markov process is a random process whose future probabilities are determined by its most recent values, depending on the order of the process. It can be considered as a process which, at any time, is in a distinct state selected from a set of N states $S_1, S_2, \ldots, S_N$. As time passes, the process either faces a change in its state or remains in the preceding state. In a Markov process, each state corresponds to a distinct, observable physical output. On the other hand, in a hidden Markov model, the observations are probabilistic functions of the states: in each state, all observations are possible, but with different probability levels. In this case, the resulting model is based on a doubly embedded stochastic process in which the underlying stochastic process is not observable (it is hidden), but can be tracked through the other stochastic process that produces the sequence of observations.

The elements of an HMM are: N the number of hidden states (in some applications there is no clear physical meaning to the states), $A = \{a_{ij}\}$ the distribution of the states transition probability, M the number of definite observation symbols (i.e. observation symbols are distinct observable physical outputs), $B = \{b_j(V)\}$ the distribution of observation symbol probability, and finally π the initial state distribution. Fig. 2 illustrates a three state hidden Markov model ($N = 3$). Arrows represent state transitions. The probability of each transition from state S_i to state S_j is denoted by a_{ij}. In this illustration, there are three observation symbols ($M = 3$). Each symbol, $V = v_1, v_2, v_3$, can be observed within each state. The probability of observing the various symbols within a given state S_j is given by $b_j(V)$ and is indicated with a bar plot. These parameters can be presented in the short form $\lambda = (A, B, \pi)$, which is called the model.

In implementing an HMM, the observations are either composed of discrete symbols such as those depicted in Fig. 2, or they are continuous, in which case they are described by probability distribution functions (so-called 'mixtures'). Models based on discrete observation symbols are referred to as discrete hidden Markov models (DHMM). Models based on continuous observations are referred to as continuous hidden Markov models (CHMM). In CHMMs, the probability distribution of observations $B = \{b_j(V)\}$ accounts for the distribution of M different mixtures in N different states. In the present paper, CHMMs are used to model two-phase flows.

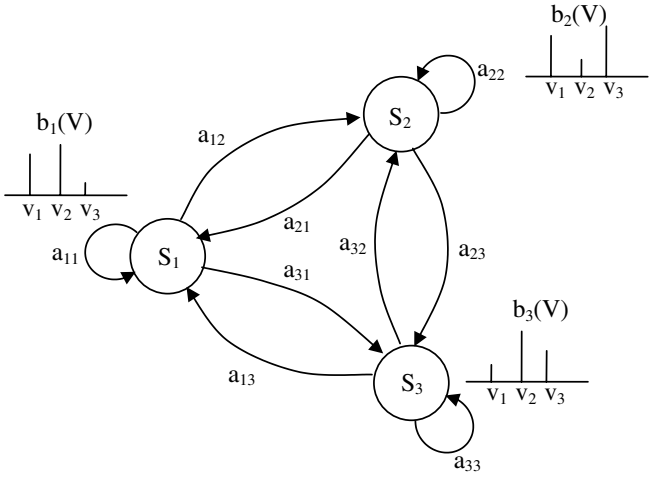

Fig. 2. A schema of a three state hidden Markov model.

The implementation of CHMMs is achieved in two dominant steps. The first step is called training. The purpose of training is to build a CHMM out of a given signal. Specifically, model parameters $\lambda = (A, B, \pi)$ are iteratively adjusted to maximize the probability of observing that signal. That is to say, given an observation sequence $O = o_1, o_2, \ldots, o_T$, the appropriate values of model parameters $\lambda = (A, B, \pi)$ are mathematically calculated such that the probability of observation sequence O given the model λ (i.e. $P(O|\lambda)$) attains its maximum value. The second step is called identification. The purpose of identification is to calculate the probability of observing a signal, given a pre-trained CHMM. In this step, the probability of observing any sequence O, given a predetermined CHMM can be mathematically estimated. That is to say, if the parameters of a CHMM are already calculated based on an observation sequence, then the similarity of such observation sequence to any other observation sequence can be quantified. This feature makes CHMM a very strong tool for comparing two or more signals and is a key to solve several problems in practice.

In the following sections, two-phase flow measurements and CHMM implementation will be described and flow regime identification using CHMMs will be discussed.

4. Experimental and data acquisition procedure

In order to gather instantaneous local fluid phase signals required in CHMM implementation, 60 conditions (Table 1) were simulated in a test section. The air–water two-phase vertical upward flow consisted of seven homogeneous velocities (0.5–5 m/s) and nine void fractions (10%–90%). In the test section (Fig. 3), air and water were fed into a mixer. The resulting two-phase mixture entered from the bottom end of a transparent polycarbonate tube with 2 m long and 19 mm of inside diameter. The pipe was mounted vertically using clamps at both ends of the tube. The mixer was installed in a way that air entered with an angle of 45°

Table 1
Test numbers, and two-phase flow conditions simulated in test section

Homogeneous flow velocity (m/s)	Homogeneous void fraction (%)								
	10	20	30	40	50	60	70	80	90
0.5	1	2	3	4	5	6	7	8	9
1	10	11	12	13	14	15	16	17	18
1.5	19	20	21	22	23	24	25	26	27
2	28	29	30	31	32	33	34	35	36
3	37	38	39	40	41	42	43	44	45
4	46	47	48	49	50	51	52	53	54
5	–	55	56	57	58	59	60	–	–

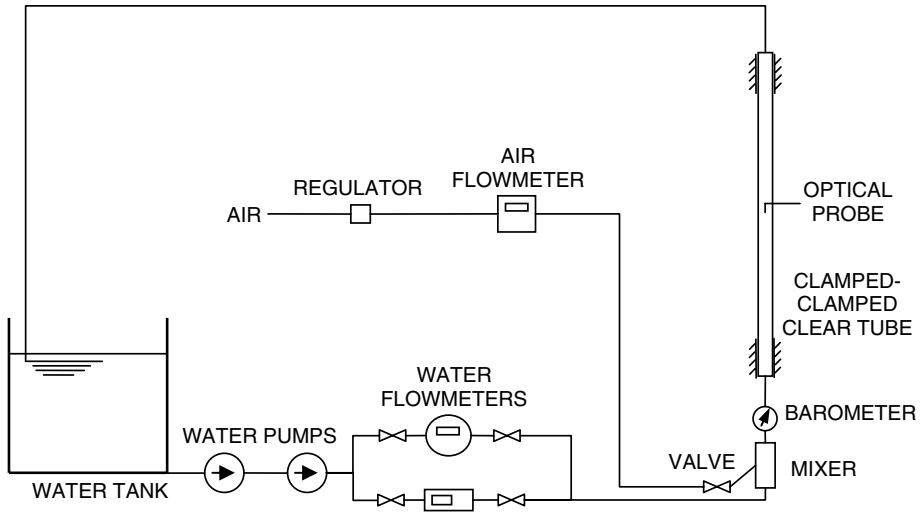

Fig. 3. Experimental setup.

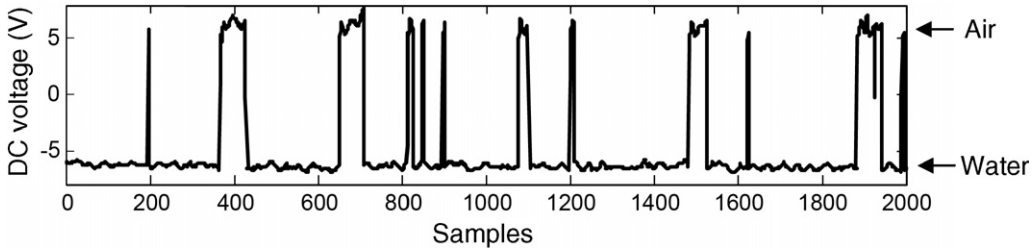

Fig. 4. An example of the measured signal using optical fiber probe.

and water with an angle of 90° with respect to tube center line. The mixer was equipped with a barometer that measured the pressure of the mixture at the entrance of the transparent tube.

The air was supplied at room temperature from the main line in the laboratory. The airflow rate was measured by an Omega (FMA-A2322) electronic mass flowmeter. The flowmeter had an accuracy of 1% of full scale (i.e. in a range of 0.85–75 SLPM). The airflow rate was compensated iteratively, with respect to the pressure measured at the tube entrance. The water was supplied at room temperature from a constant head tank to the mixer using two pumps that were arranged in series. One pump was used only for low flow rates and the other one for higher flow rates. Two different flow meters were used for measuring high and low water flow rates. For lower flow rates, a Rosemount (9711TSA30FU5N0) magnetic flowmeter with the accuracy of 0.5% of actual flow and for higher flow rates, a blue–white (FHXX10M2) turbine flowmeter with the accuracy of 1% of full scale (i.e. in a range of 7.6–75.7 LPM) were used. Using these instruments, the simulated homogeneous flow velocities were accurate within ± 0.09 m/s. The void fractions were accurate within $\pm 4\%$, except at very low velocities (i.e. $V = 0.5$ m/s) and void fractions ($\alpha \leqslant 40\%$), for which the accuracy of void fraction was $\pm 8\%$, for all other conditions the accuracy was better than 4%.

Instantaneous local fluid phase signals were collected using a single step index multimode optical fiber probe located at the center and mid-length of the tube. This probe generates a DC voltage that depends on the reflection coefficient of the fluid in which it is immersed (Morris et al., 1987). The DC voltage signals were recorded using a National Instruments data acquisition board and LabVIEW software. For each condition simulated in the test section, 1 minute worth of data were sampled at a frequency of 99 kHz. Besides, for each test, flow patterns were captured using an E4500 Nikon digital camera at the speed of 1/2000 s and from a distance of 35 cm from the tube.

The signals produced by the optical fiber probe system comprise of two unsteady but distinguishable values (approximately $+5$ V in air and -5 V in water), as in Fig. 4. The local phase of the flow is therefore determined from instantaneous values of the signals: at each instant, a positive value denotes the presence of the gas phase, and a negative value denotes the presence of the liquid phase.

5. CHMM implementation in two-phase flow pattern recognition

The objective in using CHMM for two-phase flow identification is to use the data corresponding to two-phase flow conditions with a clearly known flow regime (i.e. conditions far away from transition regions) for training, and

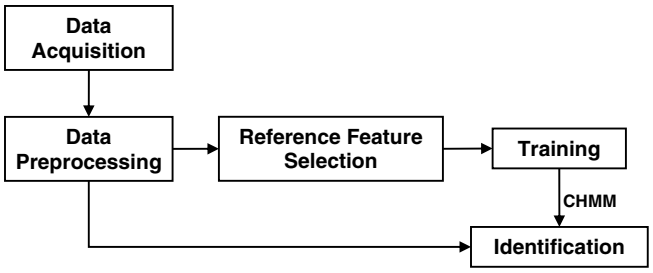

Fig. 5. CHMM implementation procedure for two-phase flow regime identification.

to detect the conditions with unclear flow regime (i.e. conditions close to transition regions) through the identification process. The general procedure of CHMM implementation is shown in Fig. 5. First, the acquired signals are converted to feature vectors (i.e. observations) through preprocessing. Afterwards, some conditions are singled out as reference conditions, and for each reference condition, a CHMM is trained out of the corresponding feature vectors. Finally, in the identification step, the feature vectors of all test conditions are compared quantitatively to those of the reference conditions by the use of pre-trained CHMMs. These steps are detailed in following sections.

5.1. Data preprocessing

Using raw instantaneous local fluid phase signals as observations in procedure of implementing CHMM is neither efficient nor applicable. Hence, the signals were preprocessed in three steps: down-sampling, feature extraction and feature vector derivation.

Down-sampling is used to attain the same spatial frequency for all test conditions by picking one data point out of every S data points. The data were down-sampled with respect to the homogeneous velocities at which they were recorded. In fact, since two-phase conditions with a variety of homogenous velocities were recorded at the same frequency (i.e. 99 kHz), the conditions with the same regime but different velocities would be recognized as being different. Down-sampling is a process subsequent to sampling, by which the sampling rate of the signal is reduced. In the present case, it results in data vectors having the same number of samples for a given length of the flow regardless of the flow velocity. The down-sampling ratios (S) for all the velocities are given in Table 2. It must be noted that since all the preprocessing steps were performed in the time domain, frequency aliasing, which can be caused by down-sampling, was not considered. Moreover, it was verified that temporal aliasing did not affect the final results, and was therefore considered negligible. The verification was carried out as follows: features were extracted directly from the 99 kHz signals (without down-sampling); these features were then down-scaled using the same ratios (S) as in Table 2. Finally, the results obtained by down-scaling (no aliasing) turned out to be in good agreement with those obtained by down-sampling, showing that temporal aliasing is negligible. The advantage of using down-sampling over down-scaling is the execution time.

Table 2
Down-sampling ratios for different homogeneous flow velocities

Velocity (m/s)	Desired frequency (Hz)	Down-sampling rate (theory)	Down-sampling rate (real)	Obtained frequency (Hz)	Length of flow between two samples (mm)
0.5	2000	49.5	50	1980	0.2525
1	4000	24.75	25	3960	0.2525
1.5	6000	16.5	17	5823	0.2575
2	8000	12.375	12	8250	0.2424
3	12,000	8.25	8	12,375	0.2424
4	16,000	6.18	6	16,500	0.2424
5	20,000	4.95	5	19,800	0.2525

After down-sampling, in order to have an enhanced signal interpretation, signal features were extracted. Feature extraction is aimed to highlight specific characteristics of the signal and represent it in a way suitable for signal processing. Moreover, it reduces the size of the data so as to avoid slowing down the CHMM computations. In this research, an innovative approach was used for extracting features based on the passage length of the liquid and gas phases. This approach can be explained as follows: the number of samples corresponding to the passage of a distinct mass of gas phase across the probe is recorded as a positive number with the index of the phase change. In a similar manner, the number of samples corresponding to the passage of a distinct mass of liquid across the probe is recorded as a negative number (Fig. 6). In order to

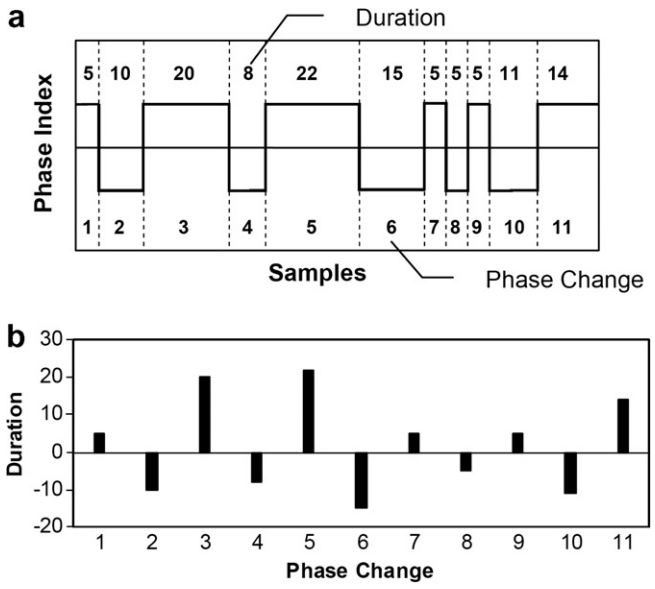

Fig. 6. Feature extraction based on the passage length of each phase: (a) down-sampled data and (b) resulting features.

specify the phases, the zero line was used as a threshold. If passage lengths are too dispersed, the logarithm of the absolute values can be used.

Since the number of samples is set to correspond to the length of the flow, passage based features get values that are proportional to the length of distinct masses of gas or liquid through the probe. Moreover, given that the lengths of such distinct masses of gas and liquid are not discrete values chosen from a predetermined set, the features (or precisely the observations) are continuous. Therefore, in order to train such observations, continuous hidden Markov models must be used. In this case the features can be treated either vectorially or individually. In most applications, vectors are preferable to single observations, due to their capability of bearing various information together in a short form. Therefore, in feature vector derivation, 1000 points of feature data (which represent 1000 phase changes) was divided into nine segments of 200 points which were separated with an offset of 100 points. Then, each segment was divided into 19 feature vectors of 20 points with 50% overlap. Finally, the feature vectors derived from a given segment were treated as elements of an observation sequence. These observation sequences were used in CHMM implementation.

5.2. Selection of reference features

In order to train CHMMs, features corresponding to some conditions with known regimes were selected as reference conditions among all the features. In order to select such conditions, photographs were used together with a flow pattern map provided by Taitel et al. (1980) for tubes with small diameter (i.e. $D \leqslant 5$ cm, where D is tube diameter). It must be noted that for smaller tube diameters (including 19 mm), the regime corresponding to dispersed bubbles does not exist, as Taitel et al. (1980) argued. Hence, the existing flow patterns are finely dispersed bubbles, churns, slugs and annular. Moreover, since the annular regime is easily detectable and difficult to reach with the available equipments, this regime was not studied in the present research. Therefore, the two-phase flow conditions used as reference conditions were chosen among the remaining three different regimes. Fig. 7 shows a map of the test conditions in which the points corresponding to the reference conditions are circled. For each regime, in order to cover the variations in flow condition due to velocity and void fraction (e.g. number of bubbles, size of bubbles, local velocity, void fraction distribution in tube section and suchlike), three reference conditions were selected and for each reference condition a separate CHMM was produced.

5.3. Training

Training is achieved in three steps: first, preliminary values are assigned to the model parameters $\lambda = (A, \pi, B)$, second, the initial values for model parameters are estimated

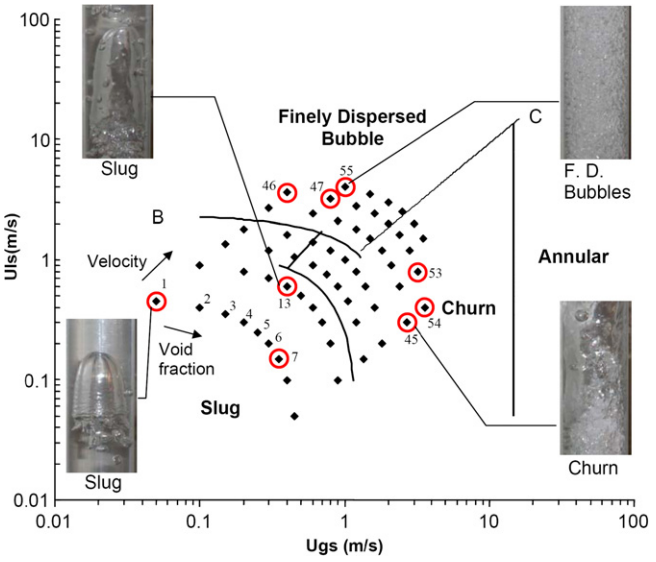

Fig. 7. Test points and reference conditions on the map of Taitel et al. (1980).

and at last, the model parameters are optimized iteratively. To assign preliminary values, the number of states ($N = 3$) and number of mixtures ($M = 1$) were first selected arbitrarily. Then with respect to the number of states and mixtures, the feature vectors were grouped into $N \times M$ clusters. In order to do so, N observations that had the greatest distance among others were selected as group centers. Euclidean distance was used to measure the distance. Then all the observations were grouped into N groups based on their proximity to the group centers. In the same way, when $M > 1$ each group would be divided into M groups using the same criterion, resulting in $N \times M$ clusters. Then the preliminary estimations of parameter B were obtained with respect to feature vectors distribution in clusters. Also, the preliminary values for initial state distribution π and the states transition probability distribution $A = \{a_{ij}\}$ were assigned a uniform value (Rabiner, 1989; Lee et al., 2004).

The next step is initial estimation using segmental k-means loop. In any iteration of this loop, the best state sequence is tracked using the Viterbi algorithm (Viterbi, 1967; Forney, 1973). The best state sequence is the sequence of successive states that is most likely to yield the maximum probability of observing a given observation sequence. The CHMM parameters $\lambda = (A, \pi, B)$ are then calculated with respect to best state sequence using the k-means clustering algorithm. This loop is iterated until a convergence criterion is met. In this research, the mean square error of all model parameters $\lambda = (A, \pi, B)$ between two consecutive iterations were summed and used as a convergence criterion. After that, the obtained initial estimates are used for re-estimating model parameters by means of an iterative procedure called the Baum–Welch method. In this step, which is the main step of the training, the model parameters are optimized so that the probability of the

Table 3
Likelihood results for condition number 14

Reference conditions	Slug			Finely dispersed bubble			Churn		
	1	7	13	46	47	55	45	53	54
Log-likelihood values	−1216.5	−1536.6	−523.57	−3502	−2017.5	−3359.7	−1396.5	−2622	−1450.3
Total log-likelihood values	−3276.67			−8879.2			−5468.8		

observation sequence is maximized. After each iteration, the probability of the observation sequence is calculated in terms of log-likelihood. Likelihood is the probability of observation sequence O given the model λ ($P(O|\lambda)$). Log-likelihood is the logarithm scaled likelihood. The re-estimation continues until the difference between the log-likelihood of two iterations becomes less than an error. In this project, an error equal to 1 was chosen; this value is minimal compared to the range of log-likelihood values obtained (less than 0.02%), and it allows for a reasonable execution time. Finally, the re-estimated model parameters are stored for being used in the identification step (Rabiner, 1989).

5.4. Identification

In the identification step, the probability of observing multiple sequences of feature vectors of the two-phase flow was calculated using forward-backward procedure in terms of log-likelihood and based upon the pre-trained CHMMs of reference conditions. The nine likelihood values obtained for each condition were used to categorize the conditions into three groups pertaining to the three flow regimes. In order to do so, the total log-likelihood values of each condition were obtained by adding up the log-likelihood values corresponding to the same reference flow regime. Then, for each condition, the regime for which the total likelihood value was greatest among the three totals was recognized to be the actual regime. As an illustration, the likelihood results of condition number 14 are shown in Table 3. As shown, the maximum total likelihood corresponds to the slug category. Therefore, the slug regime was considered for this condition. Using the same criterion, all the conditions were classified and the regime boundaries were extracted.

6. Results and analysis

In order to have a judgment, the obtained boundaries were depicted versus gas and liquid superficial velocities (U_{gs} and U_{ls}) and reported on the corresponding Taitel flow map. It must be noted that most transition boundaries suggested in the literature have regular and undistorted shape when mapped with respect to superficial velocities. This holds for both theoretical and empirical based methods. As shown in Fig. 8, the resulting boundaries from the CHMM method (i.e. the dashed lines on the map) have a reasonably regular and smooth shape, as expected. Further, the obtained boundaries are in good agreement with the photographs, though they have dissimilarities with Taitel's boundaries (i.e. solid lines). A good example for this case is condition number 22. According to Taitel's map, this condition belongs to the churn region, while the photo shows slugs. One reason for having such considerable mismatch between photos and Taitel's map is that Taitel's map was derived based mostly on theoretical concepts and may not necessarily account for all experimental factors. Another reason for that can be sought in the experimental setup. If the mixer does not mix the two phases evenly, unexpected changes in flow regime can happen. In addition, it will be discussed in the next section that the optical fiber measuring method is not free of error.

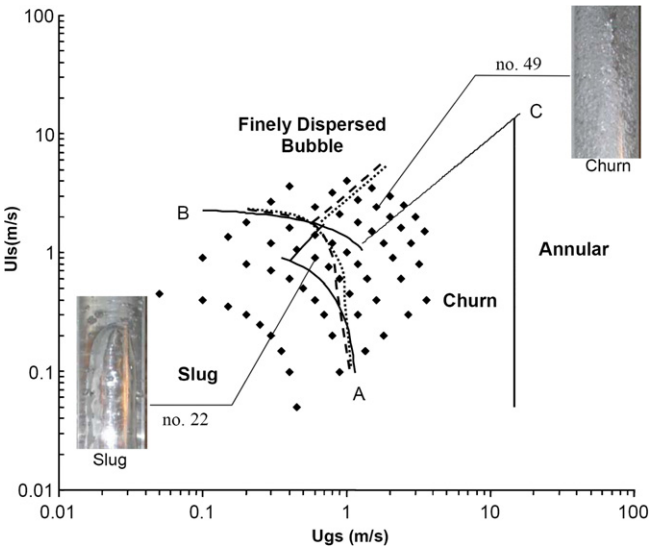

Fig. 8. Resulting map of using different number of states: (. . .) $N = 5$; (- - -) $N = 2$, 3 and 7.

In order to examine the effect of CHMM parameters, CHMMs with different numbers of states (N) and mixtures (M) were tried. In fact, N and M are the only adjustable parameters of a CHMM. Further, for any number of mixtures greater than one ($M > 1$), regardless of the number of states, the CHMM training step faced an underflow problem during execution. As a result, this parameter was kept equal to unity (i.e. $M = 1$) while the number of states was changed. As mentioned previously, the states of a CHMM may not be related to any physical interpretation, as is the case in this research. Therefore, it would be incorrect to deduce that the number of states (N) in the CHMM was given the same value as the number of possible flow

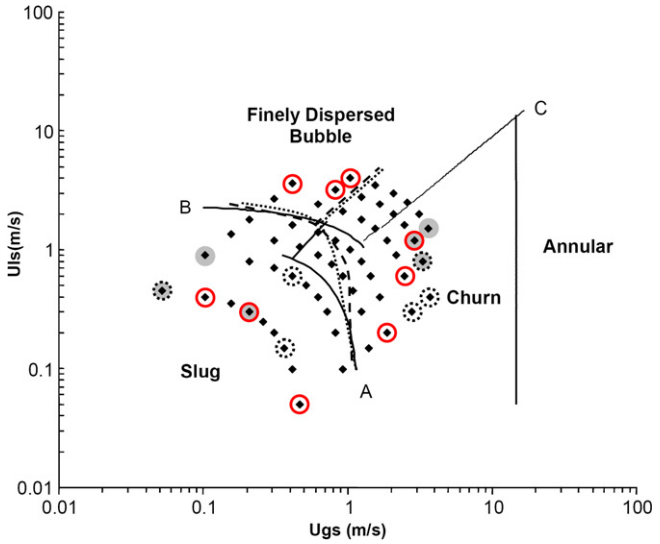

Fig. 9. Resulting map of using different reference conditions ($N = 3$): (⋯) first, (○) second and (●) third sets of reference conditions; transition borders from (···) first and third, and (- - -) second set of reference conditions.

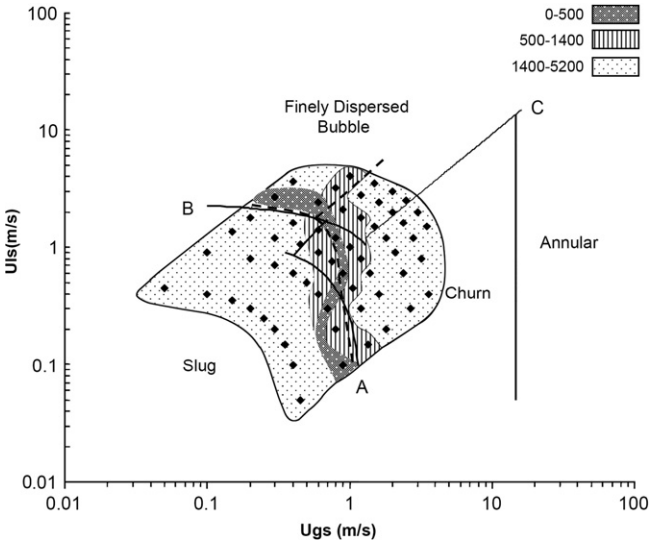

Fig. 10. Transition borders and confidence regions from a three state CHMM on Taitel's map.

regimes. Fig. 8 shows the transition boundaries obtained for $N = \{2, 3, 5, 7\}$. Transition borders are identical when using 2, 3 or 7 states. Actually, no significant change can be observed for any number of states. In fact, a model with more states is theoretically supposed to show more accurate results; however, this assumption is not necessarily true in practice (Rabiner, 1989). In the present work, models with more states do not bring any noticeable changes: it can be construed that models with few states are capable of properly represent their corresponding signals.

Furthermore, the results of using three different sets of reference conditions were considered. It must be noted that this change was made for the slug and the churn regions only. For the finely dispersed bubbles region, because of the limited number of conditions in this region, the previous reference conditions were maintained (Fig. 9). As shown in Fig. 9, there are slight variations in the obtained boundaries due to selecting different reference conditions. Therefore, it was concluded that, on the one hand changing reference conditions can affect the results, although on the other hand the change is minor as long as the reference conditions are selected not too close to the transition boundaries.

7. Confidence evaluation

In order to study the confidence of the results, the 'confidence difference' was defined as the difference between the two largest values among the log-likelihood values obtained by comparing a given flow condition with reference conditions. According to this definition, a large confidence difference shows that the condition bears exclusively the characteristics of the given regime. On the contrary, a small difference will show that the characteristics of the flow are almost equally comparable to two different regimes. Fig. 10 shows a map on which the condition points are classified into three regions with respect to their confidence difference. The confidence differences were calculated using the results of the three state CHMMs ($N = 3$). As shown, the conditions with higher confidence difference (ranged 1400–5200) are mostly those located away from the transition boundaries obtained using CHMMs. Close to transition boundaries, the confidence is low. This coincides with the fact that near transition boundaries, two phase flow bears the characteristics of both regimes between which transition occurs and accordingly, the confidence difference is low. Therefore, the boundaries obtained using the CHMM method are reasonably accurate.

One peculiarity on this map is that most conditions in the finely dispersed bubbles region have a low confidence difference. This can be explained from the optical probe measuring system. If a group of very small and closely packed bubbles crosses the probe, it will possibly be misinterpreted as a mass of air. In fact, when two bubbles are very close, the liquid film between them is very thin so that the passage time of such film is less than the summation of the signal's rising and falling time (Fig. 11). Therefore, the change in phase corresponding to the passage of the liquid film is not recorded completely, i.e. the signal does not cross the zero threshold. The passage of closely packed bubbles can happen in the finely dispersed bubbles regime. As a result, such signal has similarities with the slug or churn flows. Thus, conditions in the finely dispersed bubbles region are detected as such, but they show relatively high log-likelihoods with the churn or slug reference conditions, causing low confidence levels. Moreover, this inaccuracy can be considered as a cause for having such remarkable difference in the obtained boundary between

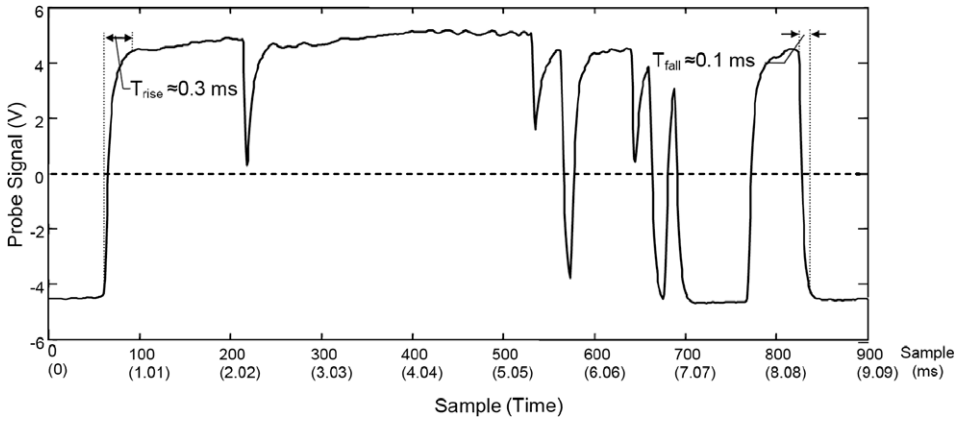

Fig. 11. An interval of the raw time signal (recorded at 99 kHz) of condition number 46.

the churns and finely dispersed bubbles regions compared to Taitel's boundary.

8. Conclusion

In this research, the practicability of hidden Markov modeling in identifying two-phase flow regimes was investigated. Also, an innovative feature extraction method was developed based on the passage length of the liquid and gas phases. The transitions boundaries obtained using CHMM were in very good agreement with photos taken during the experiments, even though there were some disagreements with the Taitel et al. map. Moreover it was observed that the number of states does not cause significant changes in the shape or location of the transition boundaries, suggesting that a model with two states ($N = 2$) and one mixture ($M = 1$) is suitable for this case. In a similar way, the choice of reference conditions does not bring about significant changes, as long as they are selected sufficiently far from transition boundaries. Furthermore, the confidence study on the results showed that the confidence near the transition boundaries is lowest, which demonstrates that there is a concordance between the results and the physical significance of the flow regime transitions.

In conclusion, it can be stated that hidden Markov model, which has been proven to be a very strong pattern identifier in different fields of engineering, has a good potential in identifying two-phase flow patterns. This research can be considered as a leading trial to many follow-ups that can be practiced in this field.

Acknowledgements

The authors are greatly indebted to Professor Michel J. Pettigrew, Chair holder and Professor Njuki W. Mureithi, co-chair of the BWC/AECL/NSERC Chair of Fluid-Structure Interaction, for their enlightening expertise and for the use of the Chair facilities. This work was supported in part by NSERC.

References

Bunks, C., McCarthy, D., Al-Ani, T., 2000. Condition-based maintenance of machines using hidden Markov models. Mech. Syst. Signal Process. 14, 597–612.

Costigan, G., Whalley, P.B., 1997. Slug flow regime identification from dynamic void fraction measurements in vertical air–water flows. Int. J. Multiphase Flow 23, 263–282.

Das, R.K., Pattanayak, S., 1993. Electrical impedance method for flow regime identification in vertical upward gas–liquid two-phase flow. Meas. Sci. Technol. 4, 1457–1463.

Ertunc, H.M., Loparo, K.A., Ocak, H., 2001. Tool wear condition monitoring in drilling operations using hidden Markov models. Int. J. Mach. Tools Manufact. 41, 1363–1384.

Forney Jr., G.D., 1973. VITERBI ALGORITHM. Proc. IEEE 61, 268–278.

Hannaford, B., Lee, P., 1991. Hidden Markov model analysis of force/torque information in telemanipulation. Int. J. Robot. Res. 10, 528–539.

Jones, O.C., Zuber, N., 1975. The interrelation between void fraction fluctuations and flow patterns in two-phase flow. Int. J. Multiphase Flow 2, 273–306.

Kelessidis, V.C., Dukler, A.E., 1989. Modeling flow pattern transitions for upward gas–liquid flow in vertical concentric and eccentric annuli. Int. J. Multiphase Flow 15, 173–191.

Lee, J.M., Kim, S.J., Hwang, Y., Song, C.S., 2004. Diagnosis of mechanical fault signals using continuous hidden Markov model. J. Sound Vibr. 276, 1065–1080.

Morris, D., Teyssedou, A., Lapierre, J., Tapucu, A., 1987. Optical fiber probe to measure local void fraction profiles. Appl. Opt. 26, 4660–4664.

Ocak, H., Loparo, K.A., 2005. HMM-based fault detection and diagnosis scheme for rolling element bearings. J. Vibr. Acoust. Transact. ASME 127, 299–306.

Rabiner, L.R., 1989. A tutorial on hidden Markov models and selected applications in speech recognition. Proc. IEEE 77, 257–286.

Rouhani, S.Z., Sohal, M.S., 1983. Two-phase flow patterns: a review of research results. Progr. Nucl. Energ. 11, 219–259.

Taitel, Y., Borena, D., Dukler, A.E., 1980. Modeling flow pattern transitions for steady upward gas–liquid flow in vertical tubes. AIChE J. 26, 345–354.

Vince, M.A., Lahey Jr., R.T., 1982. On the development of an objective flow regime indicator. Int. J. Multiphase Flow 8, 93–124.

Viterbi, A.J., 1967. Error bounds for convolutional codes and an asymptotically optimum decoding algorithm. IEEE Trans. Informat. Theory IT-13, 260–269.

Wang, L., Mehrabi, M.G., Asibu, E.K., 2002. Hidden Markov model-based tool wear monitoring in turning. Trans. ASME. J. Manuf. Sci. Eng. 124, 651–658.